Intermetallics 117 (2020) 106667

Contents lists available at ScienceDirect

Intermetallics

journal homepage: http://www.elsevier.com/locate/intermet

A new Zr-rich intermetallic phase in an Al-14Si-3Cu-4.5Ni casting alloy with trace additions of Zr

Min-Su Jo [a,b], Young-Hee Cho [a,*], Jung-Moo Lee [a], Su-Hyeon Kim [a], Jun-Yun Kang [a], Jae-Gil Jung [a], Soo-Bae Kim [a,c], Jae-il Jang [b]

[a] Division of Metallic Materials, Korea Institute of Materials Science, Changwon, 51508, South Korea
[b] Division of Materials Science and Engineering, Hanyang University, Seoul, 04763, South Korea
[c] Department of Materials Science and Engineering, Yonsei University, Seoul, 120-749, South Korea

ARTICLE INFO

Keywords:
Al-Si casting alloy
Multicomponent
Zr-rich intermetallics
Microstructure characterization
High temperature mechanical properties
Nucleation

ABSTRACT

A trace addition of Zr to a multicomponent Al-14Si-3Cu-4.5Ni casting alloy has often been found to form a coarse plate-like Zr-rich intermetallic compound with a size of a few tens of μm at the beginning of solidification. Evaluation of the phase composition has confirmed that the Zr-rich intermetallic phase consists of multicomponent constituent elements, mainly Al, Si, Ni and Fe, and is present in a form of $(Al,Si)_3(Zr,Ni,Fe)$. The existence of such a complex $(Al,Si)_3(Zr,Ni,Fe)$ phase has not yet been predicted by phase equilibria calculation of the multicomponent Al-14Si-CuNiMg systems. In this paper, transmission electron microscopy studies combined with electron backscattered diffraction pattern analysis reveals the crystallography information of the $(Al,Si)_3(Zr,Ni,Fe)$ phase for the first time and identifies it as a modified Al_3Zr-D023 crystal (tetragonal, I4/mmm(139)) with slightly changed lattice parameters of a = b = 3.275 Å and c = 15.475 Å. The primary $(Al,Si)_3(Zr,Ni,Fe)$ phase is found to nucleate directly onto AlP particles. The mechanical properties of the Zr-rich intermetallics were also investigated using nanoindentation at both room and elevated temperatures and were compared to those of the Si phase.

1. Introduction

Multicomponent Al-Si casting alloys have been widely used for high-temperature powertrain applications owing to their important characteristics: good castability, high strength-to-mass ratio, and low thermal expansion coefficients with good wear resistance. The accelerated demand for improved fuel efficiency necessitates the development of new alloys for pistons which can withstand higher gas temperatures of 350–400 °C and pressures up to 20 MPa. In order to maintain strength at the elevated temperatures, alloy design for Al-Si casting alloys has been extensively approached with the addition of substantial amounts of Cu and Ni [1–5]. Moreover, certain transition metals (TMs), such as Ti, V and Zr, have been suggested to improve high temperature performance with a strengthening mechanism associated with thermally stable precipitates and intermetallics. The transition elements have low diffusivity and solubility in Al and form Al_3TM precipitates, and tri-aluminide phases with a cubic $L1_2$ structure can maintain coherency with the Al matrix at elevated temperatures of 370–425 °C [6] and thus contribute to the high temperature strength. Meanwhile, when a TM is added to Al-Si casting alloys, Si in the alloys is likely to react with the TM and TM-rich silicides ($TMSi_2$), and Si can also dissolve into coarse flake-like tetragonal Al_3TM-$D0_{23}$ intermetallics in the early stage of solidification [7–12]. This could decrease the amount of solute retained within the Al matrix [13] and thus reduce the volume fraction of thermally stable Al_3TM- $L1_2$ precipitates. Owing to their stable nature at 350 °C, however, Gao et al. [8,11,14] reported that Ti/Zr-rich intermetallics also significantly improved the elevated temperature properties of Al-Si piston alloys, particularly when they were formed in a blocky shape with the additions of high content Ti (3.1 wt%) or Zr (2.5 wt%). It was also proven that flake-like $(Al,Si)_3Zr$ intermetallics that formed with a trace Zr addition had a marginal or even detrimental effect on the high temperature strength [8,14].

The combined addition of Zr with Ni has been attempted in order to improve the high temperature properties of Al-Si casting alloys [8,9,14,15]. Minor additions of both Zr and Ni were designed to form such coherent precipitates as Al_3Zr-$L1_2$ and Al_3Ni in the Al matrix while

* Corresponding author.
E-mail address: y.cho@kims.re.kr (Y.-H. Cho).

https://doi.org/10.1016/j.intermet.2019.106667
Received 18 September 2019; Received in revised form 20 November 2019; Accepted 20 November 2019
Available online 28 November 2019

inevitably producing various intermetallic phases of Al_3Ni, Al_9FeNi and $(Al,Si)_3Zr$ upon solidification [9,16]. The evaluation of phase equilibria in a ternary Al-Ni-Zr predicted that the presence of Zr and Ni could form various ternary AlNiZr intermetallics of which the crystal structure varied with phase composition [17,18]. With the addition of Ni content up to 4 wt%, Belov et al. [13] reported that Zr formed no phases, excluding Al_3Zr-$L1_2$ dispersoids, in the Al-Ni-Mn-Fe-Si-Zr systems while Ni formed primary Al_9FeNi with eutectic Al_3Ni phases without interaction with Zr.

We designed new Al-Si piston alloys with variations in the content of the alloying element for high temperature applications [12,19,20]. Acknowledging that both Cu and Ni enhance load transfer to an interconnected Al-Si eutectic network by forming various Cu/Ni-containing intermetallic phases, we attempted alloying with increased Ni content in excess of the Cu amount, while microstructural refinement was achieved through liquid metal processing combined with fast cooling. In the alloy with trace additions of Ti, V, Zr, instead of forming a primary Al_3Ni phase, we experimentally observed that Ni was present in a massive flake-like Zr-containing phase that was not included in the databases of TCAL3 of Thermo-Calc [21] nor FTlite of FactSage [24]. This importantly indicates that Ni dissolved in the Zr-rich intermetallic phase and then changed the composition and the crystallography characteristics of the phase.

Therefore, the aim of this work is to clarify the formation of a new Zr-rich intermetallics in the multicomponent Al-14Si-3Cu-4.5Ni alloy. The study involves phase identification of the Zr-containing intermetallics with a combinational use of transmission electron microscopy (TEM) and electron backscattered diffraction (EBSD). The hardness of the new intermetallic phase at both room temperature and elevated temperature (350 °C) was also investigated using hot-stage nanoindentation, and its important role for high temperature strength is further discussed.

2. Experimental

The Al-14Si alloy used in this study was produced by Dong Yang Piston Co., Ltd. (Korea). The chemical composition of the alloy is given in Table 1. The alloy melt was degassed with inert gas (Ar) and was isothermally held at 800 °C. The melt weighing 2.5 kg was then cast into a steel permanent mould preheated to 130 °C at a cooling rate of 4 K/s. T7 heat treatment (solid solution treatment at 470 °C for 2 h followed by aging at 230 °C for 5 h) was carried out on the cast alloys.

Metallographic samples were prepared by a standard polishing procedure with a final polishing by a 0.05 μm colloidal silica suspension. The microstructures of the specimens were observed using a Nikon MA200 optical microscope (OM), a JEOL JSM-6610LV scanning electron microscope (SEM) and a ZEISS Merlin Compact SEM equipped with an energy dispersive X-ray spectrometer (EDS). Electron backscatter diffraction (EBSD) combined with EDS was applied to identify intermetallic phases using a JEOL JSM-7900F field emission SEM (FE-SEM) and AZtecSynergy software. A thin foil sample containing phases of interest was prepared by a JEOL JIB-4601F focused ion beam (FIB) and was analyzed by a JEOL JEM-2100F transmission electron microscopy (TEM).

The nanoindentation method was used to measure the mechanical properties derived from the measured load-displacement curves under loading/unloading through appropriate data analysis. The hardness was determined using a technique developed by Oliver and Pharr [23]. The indentation experiments were performed using a Hysitron TI-950 nano indenter. The alloy after prolonged aging at 350 °C for 100 h was machined into a plate with a uniform thickness of 5 mm and 10 mm of length and width. The sample was then carefully polished in a way similar to the EBSD sample preparation. A three-sided pyramid Berkovich tip was used for all indentations. For each phase of interest, particularly the Si phase and Zr-rich intermetallics, approximately 10 different indentations were made with a maximum load of 10 mN at a loading rate of 0.5 mN/s, followed by holding for 10 s in order to obtain reliable data. A hot stage consisting of a thermally controlled heating element and a ceramic insulator was used for indentations at elevated temperature (350 °C). To obtain thermal equilibrium, heating of the sample involved multiple steps, gradually heating to the targeted temperature of 350 °C for 30 min and holding it for another 30 min. With stable environmental conditions for the hot stage, experiments were performed in a chamber with an argon atmosphere surrounding the heated sample to prevent oxidation.

3. Results and discussion

3.1. Identification of a new Zr-rich intermetallic phase

Fig. 1 (a) shows a Scheil simulation of the Al-14Si alloy predicting the phases formed in the early stage of solidification using Thermo-Calc with a TCAL3 database [21]. Trace addition of 40 ppm P was also considered for the thermodynamic calculation using FactSage with a FTlite database [24] and the result has been subsequently implemented to the Thermo-Calc calculation. This is reasonably in good agreement with cooling curve analysis experimentally detecting the reactions of primary phases during solidification at a cooling rate of 0.3 K/s as shown in Fig. 1(b). Due to the very small volume fractions of silicides, such as Si_2Zr and Si_2Ti as well as AlP, their reactions were hardly detected in the cooling curve of Fig. 1(b). It should also be noted that Zr-rich intermetallics, of which the existence is not predicted by the thermodynamic calculation, was found to form in the early stage of solidification, even prior to the formation of primary Si as observed in both the cooling curve and the microstructure (see Fig. 2). Fig. 2(a) shows a typical microstructure of the Zr-rich intermetallics observed in the as-cast Al-14Si alloy, exhibiting a coarse plate-like morphology with a size of a few tens of μm. As shown in Fig. 2(b) and (c), EDS mapping along with point analysis on the phase in Fig. 2(a) reveal that the Zr-rich intermetallics contain large quantities of Al, Si and Ni (~51 at.%Al, ~18 at.%Si, ~23 at.%Ni) with approximately 5 at.%Zr and 3 at.%Fe. In the presence of a high Ni content of 4.5 wt%, Zr is not solely present in forms of Al_3Zr-$D0_{23}$ or Al_3Zr-L_1 phases [8,9,13,14,25] but is likely to react with Ni and Al, forming a more complex phase with additional solubility for Si and low Fe. The chemical composition quantitatively analyzed for the Zr-rich intermetallics suggests that the phase belongs to the chemical formula of $(Al,Si)_3(Zr,Ni,Fe)$.

Phase identification of constituent phases in the alloy was accomplished by combining EDS and EBSD. While analyzing constituent elements of phases by EDS, EBSD patterns were simultaneously collected to assist in the selection of a phase from a list of candidate phases derived from the crystallographic database filtered by the chemical information. Besides the open crystal structure database provided by the AZtec software (Inorganic Crystal Structure Database), the information of some excluded phases having additional solubility for different elements were also manually added for a more accurate analysis. Fig. 2(a) shows the area of scanning. It is evident from Fig. 2(d) that the EBSD phase mapping by combining EDS and EBSD was able to identify Al, Si, Al_9FeNi and $Al_3(Cu,Ni)_2$ phases based on the crystallographic information [26] as listed in Table 2. However, the Zr-rich $(Al,Si)_3(Zr,Ni,Fe)$ phase did not match any of the phases within the considered database, suggesting that

Table 1
Chemical composition of an Al-14Si-3Cu-4.5Ni alloy.

element	Si	Cu	Ni	Mg	Fe	Mn	Zr	Ti	V	P	Al
[wt.%]	14.26	3.01	4.56	0.60	0.40	0.19	0.20	0.11	0.10	0.004	bal.

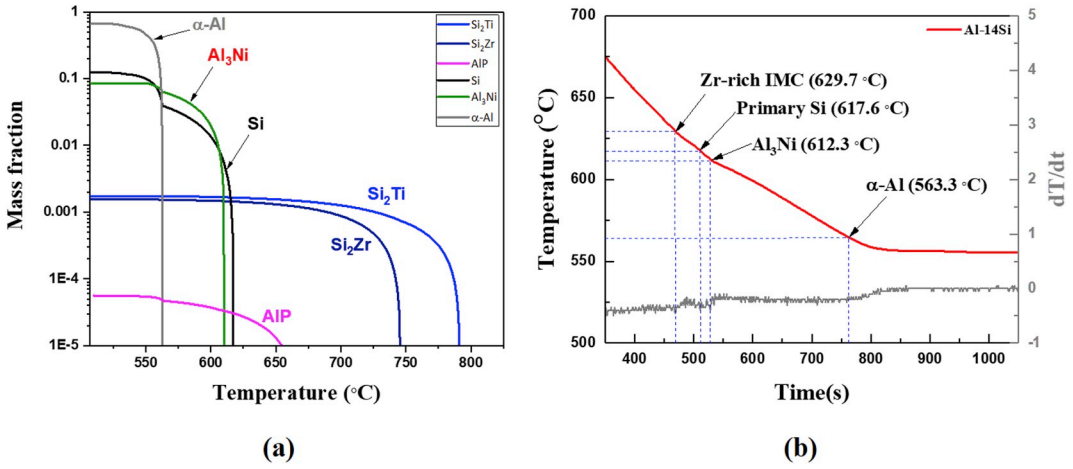

Fig. 1. (a) Scheil simulation predicting phases formed in the early stage of solidification of the Al-14Si alloy using Thermo-Calc with a TCAL3 database and (b) a cooling curve experimentally achieved during solidification of the alloy at a cooling rate of 0.3 K/s.

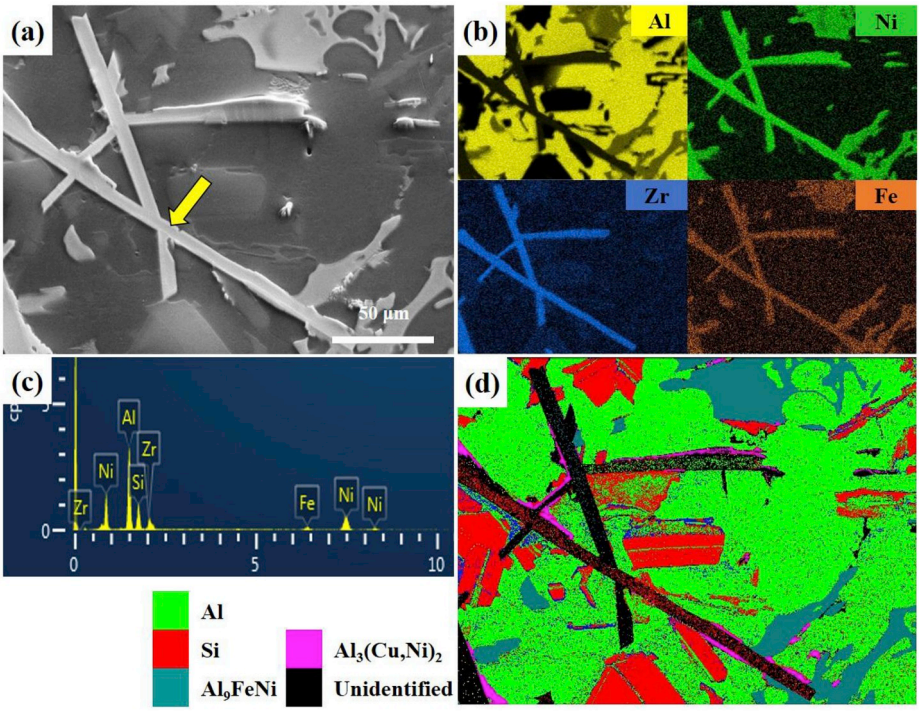

Fig. 2. (a) SEM image showing a Zr-containing intermetallic phase (arrowed) formed in the as-cast Al-14Si alloy and its corresponding (b)EDS maps exhibiting the distribution of constituent elements of the Al, Ni, Zr and Fe and (c) EDS spectrum. (d) EBSD phase map identifying Al (light green), Si (red), Al_9FeNi (dark green), $Al_3(Cu,Ni)2$ (magenta) except the Zr-containing intermetallics (black).

Table 2
Crystallographic data for constituent phases of the Al-14Si alloy [26].

Phase	Crystal structure	Space group (SG)	SG No.	Lattice parameter	Structure type
Al	cubic	$Fm\bar{3}m$	225	a = 4.050 Å	Cu
Si	cubic	$Fd\bar{3}m$	227	a = 5.431 Å	C
Al_9FeNi	monoclinic	$P2_1/c$	14	a = 6.290 Å b = 6.210 Å c = 8.560 Å β = 94.76°	Al_9Co_2
$Al_3(Cu, Ni)_2$	hexagonal	$P\bar{3}m1$	164	a = b = 4.028 Å c = 4.891 Å γ = 120°	Al_3Ni_2

a large quantity of Ni dissolved in the phase would control the lattice parameter or even the crystal structure of the known $(Al,Si)_3Zr$ phase (tetragonal, I4/mmm (139), a = 4.005 Å, c = 17.285 Å) [26].

To clarify the crystallographic information of the new Zr-rich $(Al, Si)_3(Zr,Ni,Fe)$ phase, we precisely extracted a TEM sample containing the phase using a FIB milling technique and then analyzed it for both the chemical and crystallographic information. Fig. 3(a) shows a SEM image exhibiting an $(Al,Si)_3(Zr,Ni,Fe)$ phase selected for FIB preparation of the TEM sample. Cross-sectioning across the dotted line in Fig. 3(a), we observed the $(Al,Si)_3(Zr,Ni,Fe)$ phase as shown in Fig. 3(b). Fig. 3(c) and (d) show a high resolution TEM image and an electron diffraction pattern, respectively, obtained from a squared area of Fig. 3(b). As can be seen in the inset of Fig. 3(c), the selected area diffraction pattern obtained by Fast Fourier Transformation (FFT) analysis indicates that

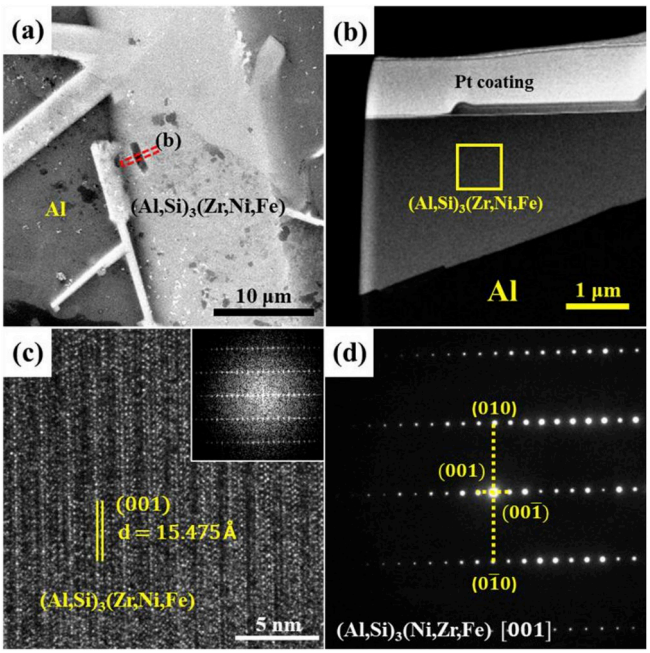

Fig. 3. (a) SEM image showing an $(Al,Si)_3(Zr,Ni,Fe)$ phase containing an internal particle in the as-cast Al-14Si alloy and (b) the cross-section image in the FIB sample. (c) HR TEM image obtained from (b) the squared area and (d) its electron diffraction pattern identifying the Zr-rich intermetallics as a new tetragonal $(Al,Si)_3(Zr,Ni,Fe)$ phase.

the c-axis [001] is normal to the plane of the $(Al,Si)_3(Zr,Ni,Fe)$ plate of which the growth is likely to occur with a strong anisotropy. This is in good agreement with the primary Al_3Zr crystals of which the {001} planes are known to have a high crystalline perfection and thus make it too difficult for atoms to attach to these planes during the growth process [27]. Further analysis on the SAD pattern in Fig. 3(d) confirms that a unit cell of $(Al,Si)_3(Zr,Ni,Fe)$ can be described as a body-centered tetragonal (I4/mmm) with lattice parameters of 3.275 Å and 15.475 Å for a and c, respectively. It should also be mentioned that Ni and Fe can certainly replace Zr in $(Al,Si)_3Zr$ but they are unlikely to change the crystal structure. However, a high content of Ni of ~23 at.% (and a few Fe) dissolved in the $(Al,Si)_3(Zr,Ni,Fe)$ and otherwise controlled the lattice parameters, reducing both the a and c values by 18% and 10%, respectively.

The experimentally determined crystallographic file for $(Al,Si)_3(Zr,Ni,Fe)$ was implemented in the crystallography database and manual EBSD analysis was once again carried out. As can be seen in Fig. 4, it should be highlighted that the Kikuchi diffraction patterns in Fig. 4(b) are consistent with the $(Al,Si)_3(Zr,Ni,Fe)$ intermetallics. This importantly suggests that the $(Al,Si)_3(Zr,Ni,Fe)$ is indeed a new intermetallic Zr-rich phase that is significantly different in chemical composition and

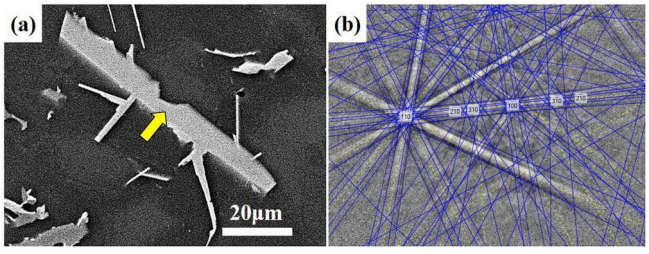

Fig. 4. (a) SEM images showing an $(Al,Si)_3(Zr,Ni,Fe)$ intermetallic phase in the as-cast Al-14Si alloy and (b) the corresponding EBSD diffraction pattern with simulated bands based on the crystallographic information derived from TEM analysis in Fig. 3(c) and (d).

lattice parameters compared with $(Al,Si)_3Zr$.

3.2. Formation of $(Al,Si)_3(Ni,Zr,Fe)$ intermetallics

Thermodynamic calculation [24] predicts that the addition of Ni exceeding 2.3 wt% can form primary Al_3Ni following the formation of primary Si in the investigated alloy (see electronic Supplementary Fig. S2). Ni less than 2.3 wt%, on the other hand, is more likely to form eutectic Al-Al_3Ni instead of developing primary Al_3Ni. Therefore, the addition of approximately 4.5 wt%Ni in the alloy containing 0.2 wt%Zr provides excess Ni in the melt, which makes it possible to form primary Al_3Ni while being also incorporated in the pre-existing Al_3Zr in the early stage of solidification. We experimentally confirmed that the primary tetragonal Al_3Zr intermetallics were not solely formed but were rather capable of containing substitutional solutes of Si, Ni and Fe, forming tetragonal $(Al,Si)_3(Zr,Ni,Fe)$ intermetallics as evidenced in Figs. 1 and 2.

The commercially available thermodynamic databases of TCAl3 and FTlite for Thermo-Calc and FactSage, respectively, have not yet recognized the formation of the complex $(Al,Si)_3(Zr,Ni,Fe)$ intermetallic phase for Scheil simulations and thus were not likely to give an accurate prediction for the early stage of solidification as shown in Fig. 1(a). A cooling curve of the Al-14Si alloy in Fig. 1(b) clearly exhibits a reaction occurring at about 630 °C where no other phases than $(Al,Si)_3(Zr,Ni,Fe)$ could possibly form in the first stage of solidification. It was also predicted that the alloy containing 40 ppm P can have AlP formed at 667.8 °C followed by the formation of $(Al,Si)_3(Zr,Ni,Fe)$ and primary Si, which suggests that the AlP could affect the nucleation of such primary phases.

Fig. 5(a) shows a typical SEM micrograph of an $(Al,Si)_3(Zr,Ni,Fe)$ phase where an internal particle is often found to be entrapped. The squared area in Fig. 5(a) was further investigated for the EDS point analysis and line scan across the internal particle and the surrounding intermetallics as shown in Fig. 5(b). Fig. 5(c) reveals that Al and P are detected from the internal particle and O is also always present in large quantities, possibly due to the active reaction with water during conventional polishing process. The EDS line scan results in Fig. 5(d) further confirm the presence of Al and P within the particle, suggesting that the AlP particle can act as a potent nucleation site for $(Al,Si)_3(Zr,Ni,Fe)$ intermetallics. Such an intimate physical relationship between the phases however does not provide conclusive proof of nucleation and hence the crystallographic evidence needs to be proved by means of TEM. On a TEM sample prepared by FIB milling to extract $(Al,Si)_3(Zr,Ni,Fe)$ intermetallics containing AlP (see electronic Supplementary S.2), we therefore attempted to look further into the internal interfaces between AlP and $(Al,Si)_3(Zr,Ni,Fe)$. Fig. 5(e) shows a TEM image exhibiting an AlP particle well-wetted by $(Al,Si)_3(Zr,Ni,Fe)$ while the oxidation occurring on the AlP particle was observed to even be accelerated during the TEM work. This oxidation event rapidly disrupted the crystalline nature of AlP and hence the AlP contacting the $(Al,Si)_3(Zr,Ni,Fe)$ intermetallic phase was found to have a typical amorphous structure as shown in Fig. 5(f). It is known that AlP has a face centered cubic (fcc) structure and the lattice parameter is 5.431 Å. The interatomic spacing along the most closely packed direction of AlP <01-1> is 7.680 Å of which the double is nearly identical to the closely packed direction $(Al,Si)_3(Zr,Ni,Fe)$ <001> = 15.475 Å. This yields a very low lattice misfit (~2.5%) between AlP and $(Al,Si)_3(Zr,Ni,Fe)$, and thus AlP can be a potent nucleation site for the $(Al,Si)_3(Zr,Ni,Fe)$ intermetallics.

3.3. Hardness of $(Al,Si)_3(Zr,Ni,Fe)$ intermetallics

Fig. 6 (a) shows the typical load-displacement curves of $(Al,Si)_3(Zr,Ni,Fe)$ intermetallics measured at room temperature (RT) and the elevated temperature of 350 °C. For comparison, primary Si, which is known as the hardest phase in multi-component Al-Si alloys [4,5], was also investigated and the results are illustrated in Fig. 6(b). As shown in Fig. 6(a), the loading curve of $(Al,Si)_3(Zr,Ni,Fe)$ intermetallics at RT are serrated by a series of discrete steps (pop-in), indicating a process of

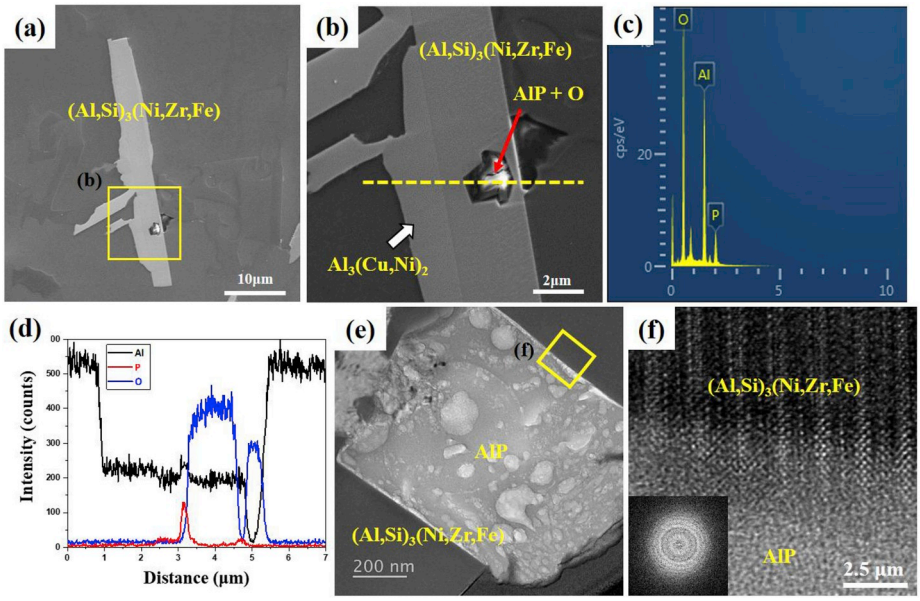

Fig. 5. SEM image showing (a) an $(Al,Si)_3(Zr,Ni,Fe)$ intermetallic phase and (b) the existence of an internal particle within the intermetallic phase in the as-cast Al-14Si alloy. (c) EDS spectrum obtained from the internal particle and (d) EDS line scan across the phases in (b) showing the presence of P and O in the centrally located particle. (e) TEM images of an $(Al,Si)_3(Zr,Ni,Fe)$ phase containing AlP particles and (e) HR TEM image showing the interface between the $(Al,Si)_3(Zr,Ni,Fe)$ and AlP as squared in (e), while exhibiting a typical amorphous structure of AlP fully oxidized, possibly $AlPO_4$.

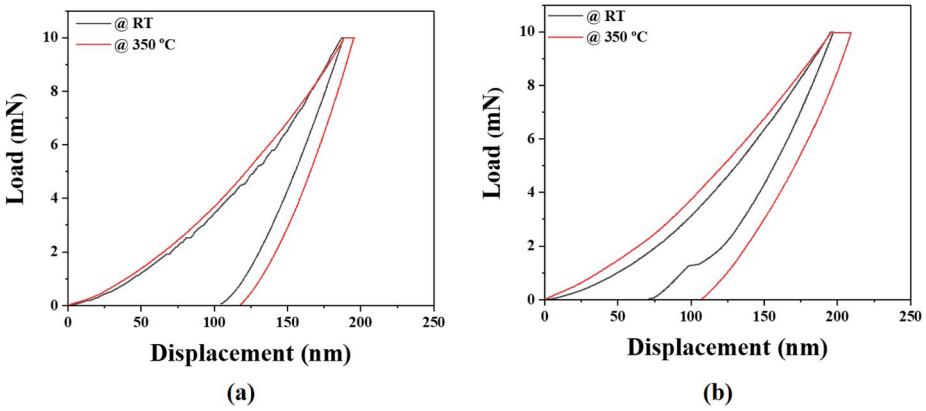

Fig. 6. Typical load-displacement curves at room temperature and elevated temperature, 350 °C for (a) $(Al,Si)_3(Zr,Ni,Fe)$ intermetallics and (b) primary Si phase.

producing mobile dislocations. Elevated temperature, however, reduces the dislocation density and allows dislocation movement. Hence, the small serrations in the loading curve disappears at 350 °C where creep effects are observed with a stable plateau occurring during the dwell time at a maximum load as shown in Fig. 6. Additionally, it appears that the hardness of $(Al,Si)_3(Zr,Ni,Fe)$ and primary Si phases are less likely to decrease with an increase in the temperature to 350 °C and both have good creep resistance.

The measured hardness of primary Si at RT is 11.0 ± 0.3 GPa, which is in good agreement with the value obtained by Chen et al. (H = 11.1 GPa) [5] and Jang et al. (H = 11.5–12.5 GPa) [28]. Primary Si exhibits a good thermal stability and maintains its hardness up to 350 °C. As shown in Fig. 6(b), the maximum indentation depth becomes slightly larger with an increasing temperature from RT to 350 °C while the gradient of the curves at both temperatures are similar. It should be noted that the measured hardness of $(Al,Si)_3(Zr,Ni,Fe)$ intermetallics is 11.3 ± 0.5 GPa, which is equivalent to that of the hard phase of primary Si at RT. As evidenced in Fig. 6(a), the change in the curve for the $(Al,Si)_3(Zr,Ni,Fe)$ intermetallics with an increasing temperature is marginal and the final indentation depth increases slightly. Average hardness values for both $(Al,Si)_3(Zr,Ni,Fe)$ and primary Si were determined by approximately 10 different indentations and the results are listed in Table 3. Similarly to primary Si, at 350 °C, $(Al,Si)_3(Zr,Ni,Fe)$ intermetallics has a small decrease of about 14% in the hardness and still retains the good high temperature stability.

Table 3
Mean hardness of $(Al,Si)_3(Zr,Ni,Fe)$ intermetallics and the primary Si phase at room temperature and 350 °C.

Hardness (GPa)	$(Al,Si)_3(Zr,Ni,Fe)$	primary Si
at RT	11.341 ± 0.464	11.018 ± 0.332
at 350 °C	9.710 ± 1.582	10.652 ± 0.475

It has been reported that the hardness of the Al matrix decreased the most drastically from 1.45 to 0.14 GPa when the temperature was increased from RT to 350 °C [5]. The softening of the matrix at the elevated temperature was due to the coarsening of Cu and Mg rich precipitates, which occurs even after a relatively short aging time of 1 h at 350 °C [29]. The high temperature strength of the Al-14Si alloy is therefore given by a transfer of load from the soft Al matrix to the rigid intermetallics, Si and the interconnected networks [3]. Introducing a large volume fraction of thermally stable intermetallics and Si may be the key to enhancing the high temperature strength of the Al-14Si alloys. Knowing that $(Al,Si)_3(Zr,Ni,Fe)$ intermetallics retains such a high hardness of about 10 GPa at 350 °C, the formation of such plate-like Zr-rich intermetallics, which allows a high degree of contiguity with Si and aluminides, can certainly contribute to the enhancement of the

elevated temperature mechanical properties. The extra load transfer from the Al matrix to the hard $(Al,Si)_3(Zr,Ni,Fe)$ intermetallics and the multiphase networks when exposed to high temperature conditions is currently under investigation and is to be further discussed in our future study.

4. Conclusions

Trace addition of Zr to a multicomponent Al-14Si-3Cu-4.5Ni alloy was found to form coarse plate-like Zr-rich intermetallics at the beginning of solidification. A detailed microstructural characterization confirmed that the formation of a $(Al,Si)_3(Zr,Ni,Fe)$ phase which had not been predicted by phase equilibria calculation of the multicomponent Al-14Si alloy.

The $(Al,Si)_3(Zr,Ni,Fe)$ intermetallics has a body-centered tetragonal (I4/mmm) structure with lattice parameters of 3.275 Å and 15.475 Å for a and c, respectively, exhibiting a modified Al_3Zr-D023 where substantial solutes of Si, Ni and Fe can be dissolved. The calculated atomic mismatch along the most closely packed direction of AlP <01-1> and $(Al,Si)_3(Zr,Ni,Fe)$ <001> is ~2.5%. Evidence that $(Al,Si)_3(Zr,Ni,Fe)$ intermetallics formed directly on AlP suggests that AlP can act as a potent nuclei site for $(Al,Si)_3(Zr,Ni,Fe)$ phases during the solidification of the Al-14Si alloy.

The $(Al,Si)_3(Zr,Ni,Fe)$ intermetallics has a very high hardness of 11.3 GPa, which is equivalent to the value of the hardest phase Si in the Al-14Si alloy. The $(Al,Si)_3(Zr,Ni,Fe)$ intermetallics has good mechanical properties at 350 °C with the good high temperature stability. The hardness of $(Al,Si)_3(Zr,Ni,Fe)$ intermetallics decreases slightly by 14% and retains a high hardness value of approximately 10 GPa at 350 °C.

Authorship statement

The results and discussion in this work have not been published previously and are not under consideration for publication elsewhere. The submission of the manuscript has been approved by all co-authors.

Declaration of competing interest

This work was supported by a research grant from the Fundamental Research Program of Korea Institute of Materials science (PNK6310). The authors declare that the fund was given by the Korean government and the results and discussion presented in this work have no conflict of interest.

Acknowledgements

The authors gratefully acknowledge a grant from the Fundamental Research Program of Korea Institute of Materials science (PNK6310).

Appendix A. Supplementary data

Supplementary data to this article can be found online at https://doi.org/10.1016/j.intermet.2019.106667.

References

[1] F. Stadler, H. Antrekowitsch, W. Fragner, H. Kaufmann, P.J. Uggowitzer, Effect of main alloying elements on strength of Al–Si foundry alloys at elevated temperatures, Int. J. Cast Metals Res. 25 (4) (2012) 215–224.
[2] C.L. Chen, R.C. Thomson, The combined use of EBSD and EDX analyses for the identification of complex intermetallic phases in multicomponent Al–Si piston alloys, J. Alloy. Comp. 490 (1) (2010) 293–300.
[3] Z. Asghar, G. Requena, H.P. Degischer, P. Cloetens, Three-dimensional study of Ni aluminides in an AlSi12 alloy by means of light optical and synchrotron microtomography, Acta Mater. 57 (14) (2009) 4125–4132.
[4] C.L. Chen, A. Richter, R.C. Thomson, Mechanical properties of intermetallic phases in multi-component Al–Si alloys using nanoindentation, Intermetallics 17 (8) (2009) 634–641.
[5] C.L. Chen, A. Richter, R.C. Thomson, Investigation of mechanical properties of intermetallic phases in multi-component Al–Si alloys using hot-stage nanoindentation, Intermetallics 18 (4) (2010) 499–508.
[6] K.E. Knipling, D.C. Dunand, D.N. Seidman, Precipitation evolution in Al–Zr and Al–Zr–Ti alloys during isothermal aging at 375–425°C, Acta Mater. 56 (1) (2008) 114–127.
[7] X.G. Chen, M. Fortier, TiAlSi intermetallic formation and its impact on the casting processing in Al–Si alloys, J. Mater. Process. Technol. 210 (13) (2010) 1780–1786.
[8] T. Gao, D. Li, Z. Wei, X. Liu, Evolution, microhardness of ZrAlSi intermetallic and its impact on the elevated-temperature properties in Al–Si alloys, Mater. Sci. Eng., A 552 (2012) 523–529.
[9] A.M.A. Mohamed, F.H. Samuel, S.A. kahtani, Microstructure, tensile properties and fracture behavior of high temperature Al–Si–Mg–Cu cast alloys, Mater. Sci. Eng., A 577 (2013) 64–72.
[10] S.K. Shaha, F. Czerwinski, W. Kasprzak, J. Friedman, D.L. Chen, Thermal stability of (AlSi)x(ZrVTi) intermetallic phases in the Al–Si–Cu–Mg cast alloy with additions of Ti, V, and Zr, Thermochim. Acta 595 (2014) 11–16.
[11] T. Gao, P. Li, Y. Li, X. Liu, Influence of Si and Ti contents on the microstructure, microhardness and performance of TiAlSi intermetallics in Al–Si–Ti alloys, J. Alloy. Comp. 509 (31) (2011) 8013–8017.
[12] J.-G. Jung, Y.-H. Cho, T.-Y. Ahn, J.-H. Yoon, S.-H. Lee, J.-M. Lee, Correlation between Primary Si and Silicide Refinement Induced by Ultrasonic Treatment of Multicomponent Al–Si Alloy Containing Ti, Zr, V, and P, Metals and Materials International, 2019.
[13] N.A. Belov, A.N. Alabin, Assessment of the Al–Ni–Mn–Fe–Si–Zr phase diagram for new–generation heat–resistant casting aluminum alloys, ICAA13: 13th International Conference on Aluminum Alloys 2012.
[14] T. Gao, X. Zhu, Q. Sun, X. Liu, Morphological evolution of ZrAlSi phase and its impact on the elevated-temperature properties of Al–Si piston alloy, J. Alloy. Comp. 567 (2013) 82–88.
[15] G.H. Garza-Elizondo, S.A. Alkahtani, A.M. Samuel, F.H. Samuel, Role of Ni and Zr in preserving the strength of 354 aluminum alloy at high temperature, in: J. Grandfield (Ed.), Light Metals 2014, Springer International Publishing, Cham, 2016, pp. 305–314.
[16] J. Hernandez-Sandoval, G.H. Garza-Elizondo, A.M. Samuel, S. Valtiierra, F. H. Samuel, The ambient and high temperature deformation behavior of Al–Si–Cu–Mg alloy with minor Ti, Zr, Ni additions, Mater. Des. 58 (2014) 89–101.
[17] P. Nash, Y.Y. Pan, The Al-Ni-Zr system (Aluminum-Nickel-Zirconium), J. Phase Equilibria 12 (1) (1991) 105–113.
[18] Q. Chen, L.H. Huang, H.S. Liu, F. Zheng, Z.P. Jin, Isothermal sections of Al-Ni-Zr ternary system at 850 and 1050 °C, J. Phase Equilibria Diffusion 34 (5) (2013) 390–402.
[19] J.-G. Jung, S.-H. Lee, J.-M. Lee, Y.-H. Cho, S.-H. Kim, W.-H. Yoon, Improved mechanical properties of near-eutectic Al-Si piston alloy through ultrasonic melt treatment, Mater. Sci. Eng., A 669 (2016) 187–195.
[20] J.-G. Jung, J.-M. Lee, Y.-H. Cho, W.-H. Yoon, Combined effects of ultrasonic melt treatment, Si addition and solution treatment on the microstructure and tensile properties of multicomponent AlSi alloys, J. Alloy. Comp. 693 (2017) 201–210.
[21] ThermoCalc-2015a with TCAL3 database, Accessed, https://www.thermocalc.com. (Accessed 30 July 2019).
[23] W.C. Oliver, G.M. Pharr, An improved technique for determining hardness and elastic modulus using load and displacement sensing indentation experiments, J. Mater. Res. 7 (6) (1992) 1564–1583.
[24] FactSage with FTlite database, Accessed, http://www.factsage.com. (Accessed 9 September 2019).
[25] A. Amenova, N. Belov, D. Smagulov, A. Toleuova, Perspective high strength aluminium alloys of new generation based on Al–Ni–Mn–Fe–Si–Zr system, Mater. Res. Innov. 18 (sup1) (2014) S1-50–S1-53.
[26] Pearson's Handbook Desk Edition, the second ed. ed., ASM International 1997..
[27] L. Li, Y. Zhang, C. Esling, H. Jiang, Z. Zhao, Y. Zuo, J. Cui, Crystallographic features of the primary Al3Zr phase in as-cast Al-1.36wt% Zr alloy, J. Cryst. Growth 316 (1) (2011) 172–176.
[28] J.-i. Jang, M.J. Lance, S. Wen, T.Y. Tsui, G.M. Pharr, Indentation-induced phase transformations in silicon: influences of load, rate and indenter angle on the transformation behavior, Acta Mater. 53 (6) (2005) 1759–1770.
[29] Y.H. Cho, Y.-R. Im, S.-W. Kwon, H.C. Lee, The effect of alloying elements on the microstructure and mechanical properties of Al-12Si cast alloys, Mater. Sci. Forum 426–432 (2003) 339–344.